Journal of Sound and Vibration (1998) **215**(5), 1145–1163
Article No. sv981660

SOUND POWER MINIMIZATION OF CIRCULAR PLATES THROUGH DAMPING LAYER PLACEMENT

H.-W. WODTKE
Zum Alten Feld 9, *D*-53773 *Hennef*, *Germany*

AND

J. S. LAMANCUSA
Center for Acoustics and Vibration, *The Pennsylvania State University*,
157 *Hammond Building*, *University Park*, *PA* 16802-1400, *U.S.A.*

(*Received* 24 *April* 1995, *and in final form* 3 *April* 1998)

Damping layers, widely used for noise and vibration control of thin-walled structures, can be designed to provide an optimal trade-off between performance and weight which is of particular importance in the automotive and aircraft industry. The goal of the presented work is the minimization of sound power radiated from plates under broadband excitation by redistribution of unconstrained damping layers. The total radiated sound power is assumed to be represented by the sound power radiated at the structural resonances. Resonance tracking is performed by means of single-degree-of-freedom (SDOF)-approximations based on near-resonance responses and their frequency derivatives. Axisymmetric vibrations of circular plates under several boundary and forcing conditions are considered. Frequency dependent Young's modulus and loss factor of the damping material are taken into account. Vibration analysis is based on the finite element method (FEM) while acoustic radiation is treated by means of Rayleigh's integral formula. It is shown that, starting from a uniform damping layer distribution, substantial reductions in radiated sound power can be achieved through redistribution of the damping layers. Depending on the given situation, these reductions are not only due to amplitude reductions but also to changes in vibration shapes and frequencies.

1. INTRODUCTION

Damping layers of various kinds are extensively used for noise and vibration control of thin-walled structures such as automotive body parts, aircraft panels, containers, or casings, and considerable research has been devoted to the field [1, 2]. Compared to the more modern vibration control measures, for example, active and semi-active control, they are still an attractive alternative (or supplement) for reasons of economy, simplicity, and stability. Their main purpose is to dissipate vibration energy, thereby reducing resonance amplitudes or increasing decay rates. This is achieved by incorporating materials into the damping layers that exhibit viscoelastic behavior. Most materials are polymer based but enamels are also used for high temperature applications. Recently, shunted piezoceramics have been suggested for use as a damping material [3].

There are basically two generic kinds of damping layers, unconstrained and constrained, both of which are applied to the surface of the structure to be damped (see Figure 1). Unconstrained layers consist of a single layer of viscoelastic material which is subject to

0022–460X/98/351145 + 19 $30.00/0

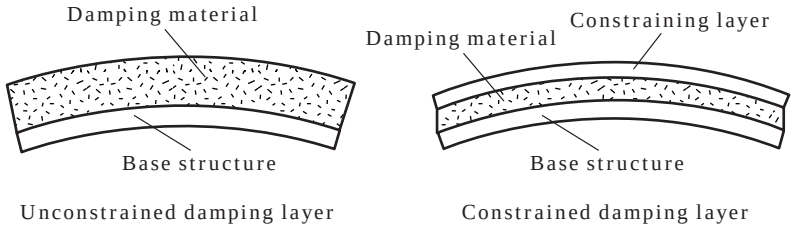

Figure 1. Types of damping layers.

tension and compression through bending of the base structure. In contrast, constrained layers force the damping material into shear by means of a constraining layer of high in-plane stiffness. While the latter, in general, are more efficient in a narrower frequency band, unconstrained layers, if applied uniformly, spread the damping effect over a wider range of wavelengths. Since unconstrained layers are easily shaped, they are attractive for shape optimization and are therefore considered in this work. However, the general approach presented can be applied to constrained layers and other vibration reduction measures as well.

Due to the nature of their action, the performance of damping layers strongly depends on their placement with respect to structural vibration shapes. For example, unconstrained layers produce the highest damping if placed at structural antinodes and, since the early recognition of this fact [4], its potential has been verified by several authors [5–8]. Various efforts were also made to redistribute the damping material in a directed fashion by using optimization techniques. Maximizing modal loss factors [9], minimizing weight for given damping and natural frequencies [10], minimizing fixed-frequency forced responses [11, 12] and minimizing resonance responses [13] are possible ways to tackle this problem. In the present work, the latter approach is used since it allows excitation properties to be taken into account while focusing on resonances where the damping takes full effect. It still allows consideration of broadband excitation as long as the overall vibration response is dominated by the resonances.

Minimization of resonance responses through structural modifications requires resonance tracking since changes of structural stiffness and mass distribution will affect the resonance frequencies. If the response calculation is based on modal superposition, the modal analysis readily provides the resonance frequencies at which the response can be evaluated. However, modal analysis is relatively expensive computationally and leads to difficulties if frequency dependent material properties are involved [14]. Therefore, direct frequency response analysis is used here, creating a min–max-problem [15] where the necessary update of the resonance frequencies after each design change is called the inner problem. This inner problem is solved by means of approximations based on single degree-of-freedom frequency responses.

Structural optimization with respect to radiated sound power can be established by minimizing the structural vibration amplitudes (e.g., minimizing the average mean square surface velocity) [16]. This purely structural approach is feasible if the acoustic wavelengths are much smaller than the structural wavelengths, in which case the radiation impedance approaches the plane-wave impedance everywhere [17]. For radiating structures subject to bending vibrations, this is fulfilled at sufficiently high frequencies. However, at lower frequencies the radiated sound power not only depends on the amplitude but also on the profile of the surface velocity as well as on the frequency. This fact can be utilized to create ''weak radiators'' by changing the structural mode shapes through variation of material properties [18], the thickness distribution [19], attached lumped masses [20] or fiber

reinforcements [21]. Since damping layers not only introduce damping but also have the potential to change vibration shapes and frequencies, it is necessary for a true low-frequency acoustical optimization to take all of those effects into account. This will be attempted in the present investigation for baffled circular plates which are relatively easily modelled yet show many effects that occur in more complicated structures.

2. PROBLEM FORMULATION

The goal of the present work is to optimize the distribution of unconstrained damping layers of limited volume on circular plates with respect to minimal radiated sound power in a given frequency band. The investigations are based on the following general assumptions.

Small deflections are considered so that linear vibration theory and acoustics can be applied.

The frequency band of excitation includes structural resonances. The damping is small enough so that the structures always exhibit distinct resonances. The resonances are well separated so that they can be recognized as single peaks in the frequency spectra.

The total power in a frequency band is represented by the power at the resonance peaks.

The base structure material as well as the damping material are homogeneous and isotropic. The material properties of the damping material are frequency dependent (temperature or other environmental influences are not considered).

The structures are embedded in an infinite plane baffle.

The impedance of the radiating structure is much higher than that of the ambient medium so that fluid loading can be neglected.

3. VIBRATION ANALYSIS

Because fluid loading is neglected, structural analysis can be treated independently from the acoustic analysis. Although the base structure considered has a simple geometry, closed form solutions cannot be used since the damping layer must be allowed to assume arbitrary distributions. Therefore, the FEM is chosen to model the base plate as well as the damping layer using 4-node axisymmetric solid elements (see Figure 2). Incompatible shape functions are introduced to prevent shear locking [22].

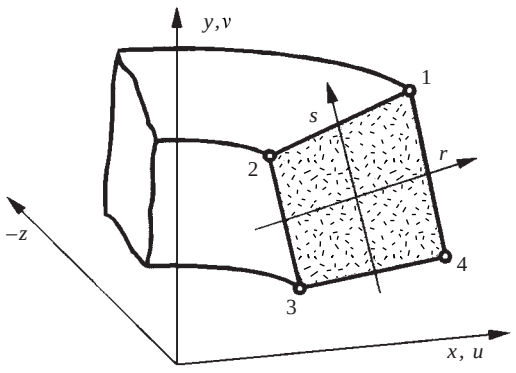

Figure 2. Axisymmetric solid element.

A two-layer damping composite is modelled by stacking the elements. Due to the formulation of the elements, what needs to be generated to model a 3-D structure is only a 2-D grid representing a radial cut through the structure. In view of the need to embed the structural analysis into an optimization procedure, a compact, stand-alone FE-program was implemented instead of using a commercial code.

Forced response analysis in the frequency domain is quite simple and readily allows for frequency dependent material properties. Damping is introduced through a complex stiffness matrix [23] (note that here, as well as in the acoustic analysis, time dependency is represented by $e^{i\omega t}$.),

$$[\mathbf{K}(\omega) - \omega^2\mathbf{M}]\mathbf{u}(\omega) = \mathbf{f}(\omega), \tag{1}$$

where $\mathbf{u}$ is the vector of nodal displacements, $\mathbf{f}$ is the forcing vector, ω is the angular frequency of excitation, $\mathbf{M}$ is the mass matrix and $\mathbf{K}$ is the stiffness matrix which is assembled as

$$\mathbf{K}(\omega) = \sum_m E_m(\omega)\mathbf{K}_m^*[1 + i\eta_m(\omega)], \tag{2}$$

where m denotes a particular material. The $\mathbf{K}_m^*$ are sub-matrices from which the frequency dependent Young's modulus, $E_m(\omega)$, and the loss factor, $\eta_m(\omega)$, have been extracted. Together with the mass matrix, these matrices are kept in memory in order to save computation time for cases where only the frequency is changed (e.g., resonance search).

In order to facilitate resonance tracking within the optimization procedure, the derivative of the vibration response with respect to frequency is needed (see section 5). Given that the vibration response itself is known, the derivative can be computed from

$$[\mathbf{K}(\omega) - \omega^2\mathbf{M}]\frac{\partial \mathbf{u}(\omega)}{\partial \omega} = \left[2\omega\mathbf{M} - \frac{\partial \mathbf{K}(\omega)}{\partial \omega}\right]\mathbf{u}(\omega) + \frac{\partial \mathbf{f}(\omega)}{\partial \omega}, \tag{3}$$

which is easily derived from equation (1). Since the left-hand side matrices of equations (1) and (3) are identical, the triangularization needs to be done only once which saves a considerable amount of computational effort.

4. ACOUSTICAL ANALYSIS

The development of numerical methods for solving acoustic radiation problems such as FEM, BEM, and Wave Superposition, has made it possible to investigate radiators of quite complex geometries. Most of these methods create a linear equation system by introducing a number of unknowns (e.g., pressures at discrete points, discrete sources) and are thus computationally quite involved. However, for plane radiators in an infinite baffle there is a relatively inexpensive solution known as the Rayleigh integral. The calculation of the sound field based on the Rayleigh integral requires only surface integrations, which makes the numerical effort considerably smaller. In view of the many evaluations occurring in an optimization loop, this is very desirable.

With reference to Figure 3 the Rayleigh integral can be formulated as

$$p(\mathbf{r}) = 2i\rho\omega \int_S v_n(\mathbf{r}_s)g(|\mathbf{r} - \mathbf{r}_s|)\, dS(\mathbf{r}_s), \tag{4}$$

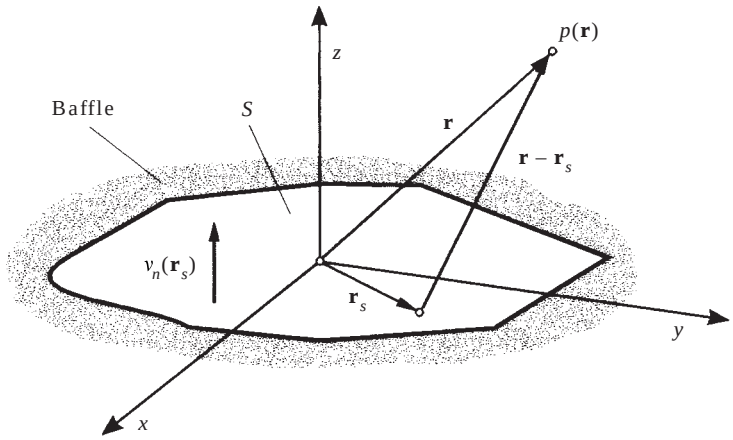

Figure 3. Plane radiator in a baffle.

where $p(\mathbf{r})$ is the acoustic pressure at field point $\mathbf{r}$, $v_n(\mathbf{r}_s)$ is the normal surface velocity at surface point $\mathbf{r}_s$, $g(|\mathbf{r}-\mathbf{r}_s|) = \mathrm{e}^{-\mathrm{i}k|\mathbf{r}-\mathbf{r}_s|}/4\pi|\mathbf{r}-\mathbf{r}_s|$ is the free space Green function, $k = \omega/c$ is the acoustic wave number, c is the speed of sound in the ambient medium and ρ is the mass density of the ambient medium.

The radiated sound power W is obtained by integrating the normal component of the time average intensity, $\mathbf{I}$, over a virtual surface that surrounds the radiator:

$$W = \int_H \mathbf{I}(\mathbf{r}_H) \cdot \mathbf{n}_H \, \mathrm{d}H = \frac{1}{2} \int_H \mathrm{Re}\,(p(\mathbf{r}_H)\mathbf{v}^*(\mathbf{r}_H)) \cdot \mathbf{n}_H \, \mathrm{d}H. \tag{5}$$

Here $\mathbf{n}_H$ is the outward normal vector of the surface. Choosing the virtual surface to coincide with the surface of the radiator and expanding the free space Green function, one obtains, from equations (4) and (5),

$$W = \frac{\rho\omega}{4\pi} \mathrm{Re}\left(\int_S v_n^*(\mathbf{r}_s) \int_{S'} v_n(\mathbf{r}_{s'}) \frac{\sin(k|\mathbf{r}_s - \mathbf{r}_{s'}|) + \mathrm{i}\cos(k|\mathbf{r}_s - \mathbf{r}_{s'}|)}{|\mathbf{r}_s - \mathbf{r}_{s'}|} \, \mathrm{d}S' \, \mathrm{d}S \right), \tag{6}$$

where the prime is used to distinguish between nested integration variables.

By using the relationship $v^*(\mathbf{r}_a)v(\mathbf{r}_b) + v(\mathbf{r}_a)v^*(\mathbf{r}_b) = 2\,\mathrm{Re}\,[v^*(\mathbf{r}_a)v(\mathbf{r}_b)]$ which holds for any pair of points (a, b), it can be shown that the cosine term does not contribute to the sound power and hence can be dropped, so that equation (6) reduces to

$$W = \frac{\rho\omega}{4\pi} \int_S v_n^*(\mathbf{r}_s) \int_{S'} v_n(\mathbf{r}_{s'}) \frac{\sin(k|\mathbf{r}_s - \mathbf{r}_{s'}|)}{|\mathbf{r}_s - \mathbf{r}_{s'}|} \, \mathrm{d}S' \, \mathrm{d}S. \tag{7}$$

This not only reduces the computational effort, but also avoids the singularity that occurs if $|\mathbf{r}_s - \mathbf{r}_{s'}| = 0$.

The radiator as well as its vibration pattern are now assumed to be axisymmetric with respect to the z-axis and to be subdivided into N rings, narrow enough that velocity and

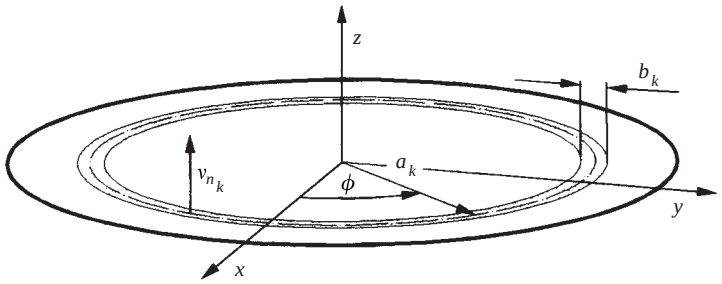

Figure 4. Discretization of the radiator surface in rings, kth ring shown.

pressure can be taken as constant over each ring (see Figure 4). Utilizing symmetry, the acoustic power is then approximated by

$$W = \rho\omega \sum_{i=1}^{N} a_i b_i v_{n_i}^* \sum_{j=1}^{i} \kappa a_j b_j v_{n_j} \int_{-\pi/2}^{\pi/2} \frac{\sin\,[k d_{ij}(\phi)]}{d_{ij}(\phi)}\,\mathrm{d}\phi, \qquad \kappa = \begin{Bmatrix} 1 & \text{if } i = j \\ 2 & \text{if } i \neq j \end{Bmatrix}, \tag{8}$$

where $d_{ij}(\phi) = |\mathbf{r}_i - \mathbf{r}_j(\phi)|$, $\mathbf{r}_i = (a_i, 0, 0)^T$ ($\phi = 0$, arbitrarily chosen), and $\mathbf{r}_j(\phi) = (a_j \cos\phi, a_j \sin\phi, 0)^T$. Equation (8) is evaluated numerically by using Gauss-integration with automatic refinement. The surface rings are chosen to coincide with the finite element discretization where the normal velocity for each ring is evaluated at the middle radius of the corresponding element surface edge.

If the wavelengths in the ambient medium are much smaller than those on the structure, which, for bending waves, holds at sufficiently high frequencies, the radiation impedance approaches ρc and the computation of the radiated power simplifies considerably:

$$\bar{W} = \rho c \int_S \frac{1}{2} v_n v_n^*\,\mathrm{d}S \approx \rho c \pi \sum_{i=1}^{N} a_i b_i v_{n_i} v_{n_i}^*. \tag{9}$$

This quantity can also serve as a measure of the overall vibration level and is later used for comparison purposes. With equation (9) the radiation efficiency can be written as

$$\sigma = W/\bar{W}. \tag{10}$$

The corresponding dB-levels are defined as

$$L_W = 10 \log (W/W_0)\,\mathrm{dB}, \qquad L_{\bar{W}} = 10 \log (\bar{W}/W_0)\,\mathrm{dB}, \qquad L_\sigma = 10 \log \sigma\,\mathrm{dB}, \tag{11}$$

where $W_0 = 10^{-12}$ W.

5. OPTIMIZATION STRATEGY

Due to the inherent complexity of the relations involved, minimization of radiated sound power forms a highly non-linear optimization problem. In this work, optimization is based on mathematical programming techniques which use problem-independent algorithms to solve iteratively a "black box" minimization task [24, 25]. A general scalar optimization problem is mathematically formulated as

$$\underset{\mathbf{x}}{\mathrm{Min}}\, f(\mathbf{x}), \qquad \mathbf{g}(\mathbf{x}) \leqslant 0, \qquad \mathbf{h}(\mathbf{x}) = 0, \tag{12}$$

where $\mathbf{x}\in\mathbb{R}^n$ is the vector of design variables, $f:\mathbb{R}^n\to\mathbb{R}$ is the objective function, $\mathbf{g}:\mathbb{R}^n\to\mathbb{R}^p$ is the vector of inequality constraints, and $\mathbf{h}:\mathbb{R}^n\to\mathbb{R}^q$ is the vector of equality constraints. In words: "Determine a set of design variables that makes the objective function a minimum and at the same time fulfills the constraints". The problem is solved by forming an optimization loop which can be divided into three parts: "structural analysis", "optimization model", and "optimization algorithm" [26]. The optimization model, described in detail below, provides the interface between the other two parts by transforming design variables into structural variables and evaluating the objective function and the constraints based on the structural and acoustic response. Out of the wide variety of algorithms that have been developed for non-linear constrained minimization a hybrid generalized-reduced-gradient/quadratic-programming method (QPRLT, [27]) is used in this work. This algorithm is one of the options included in the optimization package SAPOP [28]. It was chosen because of its good performance combined with the controllability of a line-search based algorithm. The necessary first order sensitivity information is computed via finite differences.

5.1. DESIGN VARIABLES

The thickness distribution of the damping layer is described by a polygon which forms the desired envelope to the finite elements (see Figure 5). The height of each corner point of the polygon is a design variable. The r-co-ordinates of the polygon corners are chosen at equidistant intervals where the first and the last point coincide with the boundaries (axis or rim) of the plate.

In order to allow for steep slopes, design variables may become negative. However, eliminating and recreating elements is avoided by introducing a lower limit for the element thickness, which is 1% of the thickness of the base plate.

5.2. CONSTRAINTS

The only constraint employed in this problem places an upper bound on the amount of damping material, thereby avoiding trivial solutions:

$$g_1(\mathbf{x}) = \frac{V_d(\mathbf{x})}{V_{d_{max}}} - 1. \tag{13}$$

Here, $V_d(\mathbf{x})$ is the volume of the damping layer which can be readily obtained from the FE model, and $V_{d_{max}}$ is its upper limit.

5.3. OBJECTIVE FUNCTION, RESONANCE TRACKING

The goal of the present optimization is to minimize radiated sound power over a frequency band that contains structural resonances. Strictly speaking, broadband optimization requires the objective function to be computed by integration over the frequency band. This is a computationally expensive task, especially in the presence of sharp resonance peaks and complicated radiation behavior. Therefore, it is assumed here

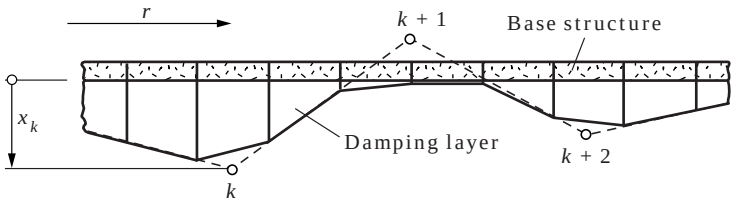

Figure 5. Design variables describing the thickness distribution of the damping layer.

that the overall radiation is characterized sufficiently by the sound power radiated at the structural resonance peaks. The objective function is then defined as

$$f(\mathbf{x}) = 10 \log \left(\sum_{k=i}^{j} 10^{(L_{W_k} - \Delta L_{A_k})10^{-1}} \right) \mathrm{dB} = L_{WA}^{i,j}, \tag{14}$$

where L_{W_k} ($L_{\overline{W}_k}$ will also be considered for comparison) is the sound power level and ΔL_{A_k} the A-weighting level-shift at the kth resonance frequency.

With this formulation, the major problem is to identify and track the resonance peaks during optimization since, generally, any modification to the structure will cause the peaks to migrate. Using modal analysis to re-identify the resonance frequencies is not only computationally intensive but encounters difficulties because of the frequency dependent stiffness matrix. Instead, an approximation technique is employed here for resonance tracking which uses SDOF-response functions to identify the resonance peaks, following the basic ideas of modal testing. From the modal representation of the vibration response,

$$\mathbf{u}(\omega) = \sum_{k} \left[\boldsymbol{\phi}_k \frac{\alpha_k + \mathrm{i}\beta_k}{1 - (\omega/\omega_k)^2 + \mathrm{i}\eta_k} \right] \tag{15}$$

($\alpha_k + \mathrm{i}\beta_k =$ modal participation factor), it is seen that at frequencies close to an eigen-frequency, ω_k, the corresponding mode-shape, $\boldsymbol{\phi}_k$, dominates the response, provided the damping is not too strong. In this case all the other modes may be combined to a vector of relatively small constants. To simplify the problem further, i.e., to obtain a linear equation system, this constant vector is also neglected leaving

$$\mathbf{u}(\omega) \approx \mathbf{q}_k(\omega) = \boldsymbol{\phi}_k \frac{\alpha_k + \mathrm{i}\beta_k}{1 - (\omega/\omega_k)^2 + \mathrm{i}\eta_k} \,. \tag{16}$$

Assuming that the response vector, $\hat{\mathbf{u}}_k$, as well as its frequency derivative, $\dot{\hat{\mathbf{u}}}_k$, at a near-resonance frequency, $\hat{\omega}_k$, is given, one can approximate the mode shape by $\boldsymbol{\phi}_k \approx \hat{\mathbf{u}}_k / \hat{u}_k$, where $\hat{u}_k$ is a suitably chosen degree of freedom (here, on the axis and perpendicular to the plate). The SDOF-parameters in equation (16) can then be determined by substituting $\hat{\omega}_k$, $\hat{u}_k$, and $\dot{\hat{u}}_k$ into equation (16) and its frequency derivative. Separating the result into real and imaginary parts and rewriting yields a linear equation system for the unknown parameters:

$$\begin{bmatrix} 1 & 0 & \mathrm{Im}\,(u) & \mathrm{Re}\,(u) \\ 0 & 1 & -\mathrm{Re}\,(u) & \mathrm{Im}\,(u) \\ \omega\ \mathrm{Re}\,(\dot{u}) & -\omega\ \mathrm{Im}\,(\dot{u}) & 0 & -2\ \mathrm{Re}\,(u^2) \\ \omega\ \mathrm{Im}\,(\dot{u}) & \omega\ \mathrm{Re}\,(\dot{u}) & 0 & -2\ \mathrm{Im}\,(u^2) \end{bmatrix} \begin{bmatrix} \alpha_k \\ \beta_k \\ \eta_k \\ (\omega/\omega_k)^2 \end{bmatrix} = \begin{bmatrix} \mathrm{Re}\,(u) \\ \mathrm{Im}\,(u) \\ 0 \\ 0 \end{bmatrix} \Bigg|_{\substack{\omega = \hat{\omega}_k \\ u = \hat{u}_k \\ \dot{u} = \dot{\hat{u}}_k}} \tag{17}$$

The resonance response is then estimated by substituting these parameters and the approximated mode shape into equation (16). Since the objective function is based on velocities rather than displacements, the response is estimated at the frequency of maximum velocity:

$$\mathbf{u}_{k_{maxV}} \approx \mathbf{q}_k(\omega_{k_{maxV}}), \qquad \text{where} \qquad \omega_{k_{maxV}} = \omega_k (1 + \eta_k^2)^{1/4}. \tag{18}$$

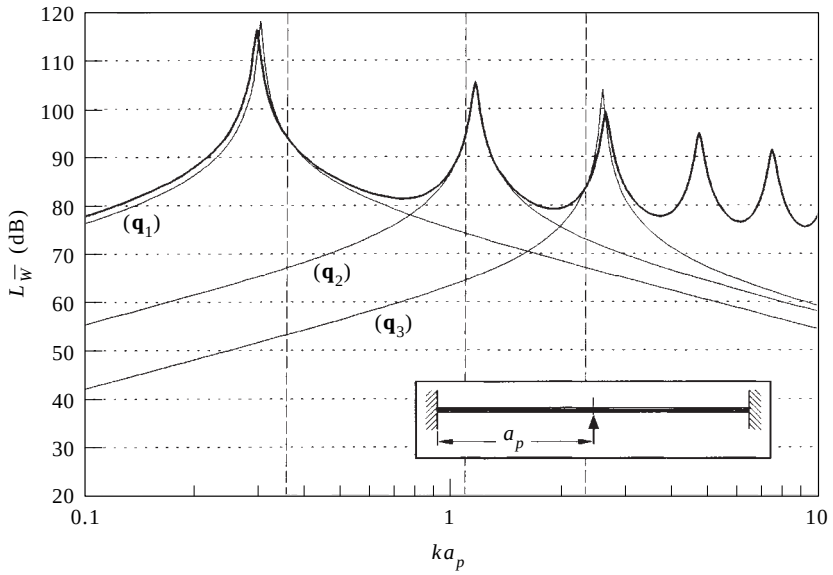

Figure 6. SDOF-approximations of the first three resonance peaks of a clamped plate, dashed verticals indicate the evaluation frequencies $\hat{\omega}_k$.

To ensure close resonance tracking the approximation process is repeated based on the true structural response at the estimated resonance frequency until a relative frequency deviation smaller than 10^{-4} is reached. At the beginning of the optimization, initial estimates for near-resonance frequencies are found by a coarse frequency sweep, whereas during the optimization process such estimates are simply taken from the previous iteration. This method yields fast convergence and behaves quite robustly since a frequency guess can be relatively far from the actual resonance (see Figure 6). Additionally, possible "jumps" to neighboring resonances can be controlled by choosing the line-search progression of the optimization algorithm appropriately. However, in cases of closely spaced resonances, strong shifts of resonance frequencies, and/or high damping, more advanced techniques such as including residuals, MDOF-curve fits, modal filtering, or pre-scanning may become necessary to ensure proper resonance tracking. If the structural changes are very small, i.e., during sensitivity analysis, updating the resonance frequencies is omitted.

6. EXAMPLES

The optimization procedure described above is applied to circular plates of three different boundary/driving conditions. Only axisymmetric vibrations will be considered, as non-axisymmetric modes always exhibit zero volume velocity and thus generally radiate weakly at low frequencies. The driving force amplitude is kept constantly 1 N over the entire frequency range. Unless stated otherwise, A-weighting is applied to the radiated sound power which is computed on the uncovered (flat) side of the plates. All plates have a radius of $a_p = 150$ mm. They are made of steel, the material properties of which are assumed to be as follows: Young's modulus, $E_s = 2{\cdot}1 \times 10^5$ N/mm^2; loss factor, $\eta_s = 0{\cdot}0$; Poisson's ratio, $\nu_s = 0{\cdot}3$; mass density, $\rho_s = 7850$ kg m^{-3}. The frequency dependent viscoelastic properties and the density of the damping layer, (see Figure 7) are measured values for Terodem® 5000 at room temperature [29] while Poisson's ratio is chosen close

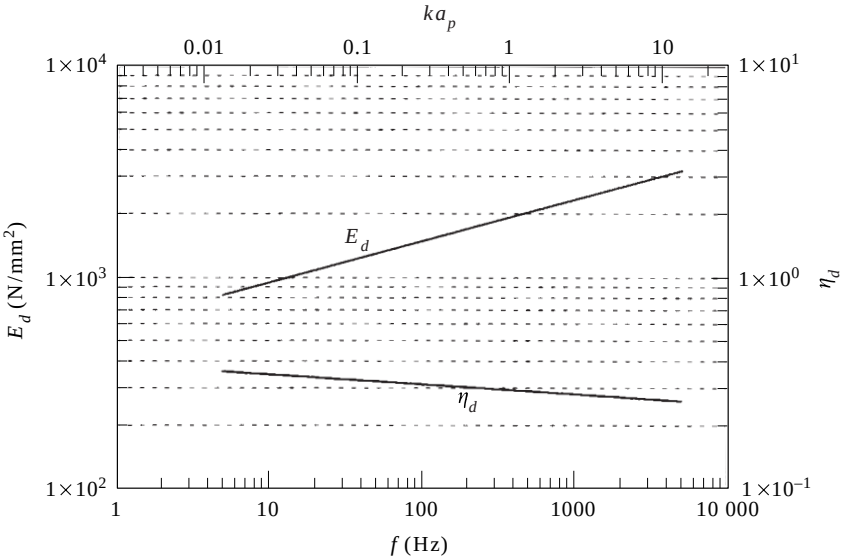

Figure 7. Frequency dependent properties of the damping material.

to 0·5 following general literature data: Poisson's ratio, $v_d = 0{\cdot}45$; mass density, $\rho_d = 1850\ \mathrm{kg\ m^{-3}}$. For the ambient medium the relevant properties are assumed to be: speed of sound, $c_a = 343\ \mathrm{m\ s^{-1}}$; mass density, $\rho_a = 1{\cdot}21\ \mathrm{kg\ m^{-3}}$.

A "baseline" plate is chosen to consist of a steel plate and a uniform damping layer each having a thickness of 1 mm. The combinations of loads and boundary conditions considered are shown in Figure 8, together with their FE-models. The base plate as well as the damping material is discretized by one layer of 50 finite elements each. To avoid a singular stiffness matrix in case of an axially free boundary (Case 2), the plate is supported by a very soft spring ($1\ \mathrm{N\ mm^{-1}}$). In Case 3, a lumped mass and a spring (both ring-shaped) are attached to the plate rim, thereby simulating the impedance of an attached structure (no rotational impedance). The mass equals 1/4 of the mass of the base plate and the spring stiffness equals the static stiffness of a simply supported base plate under uniform pressure load, evaluated at its center $(64\pi a_p^2 K(1 + v_s)/(5 + v_s)$, $K =$ plate bending stiffness).

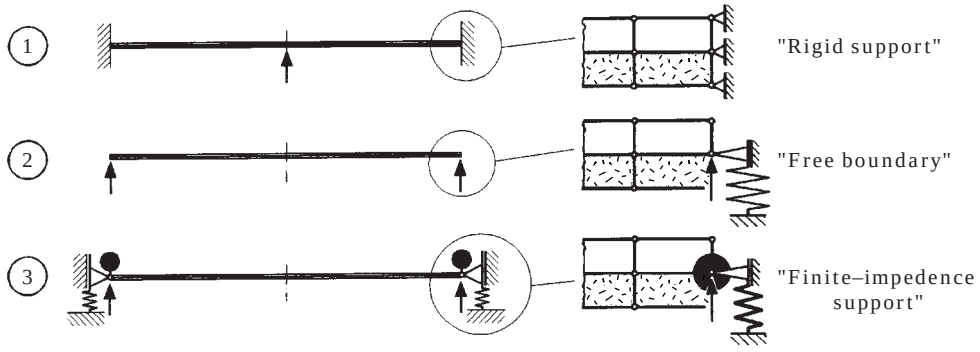

Figure 8. Combinations of load/boundary conditions, load indicated by arrows.

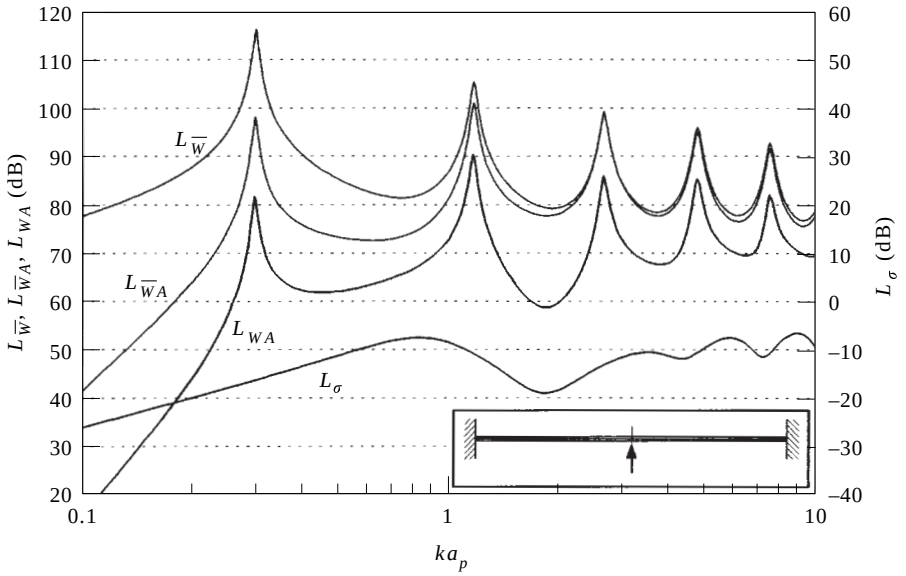

Figure 9. Acoustic frequency response functions of the clamped plate (Case 1).

6.1. GENERAL VIBRO-ACOUSTIC BEHAVIOR

Changing the damping material distribution on the plates not only alters the damping effect but also leads to different resonance frequencies and vibration shapes, thereby changing the radiation behavior in a complicated manner. Even if the damping layer is unaltered, frequencies and vibration shapes change from resonance to resonance, shifting the ratio of the structural wavelength to the wavelength in air because of the dispersive

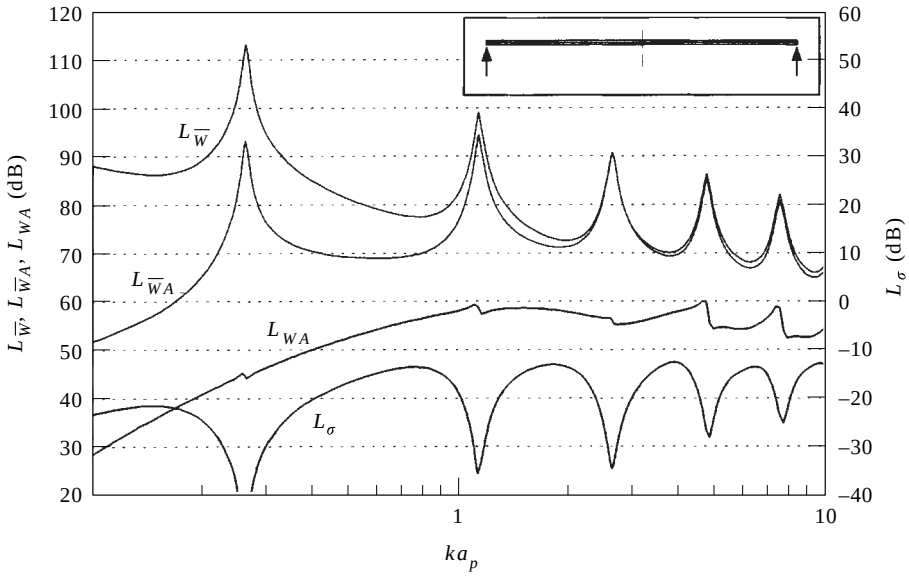

Figure 10. Acoustic frequency response functions of the free plate (Case 2).

nature of bending waves. In this way, varying the overall plate thickness (or the fluid properties) also leads to different radiation patterns.

In order to obtain an idea of the effects discussed above prior to optimization, the radiation behavior of the uniformly damped baseline plate, both with clamped and free boundary conditions (Cases 1 and 2), is investigated below. Figures 9 and 10 show the radiated sound power, with and without A-weighting, as well as the radiation efficiency and the sound power based on average mean square velocity for a frequency range encompassing the first five plate resonances.

In view of the rather obvious vibration response of the plate, expressed by $L_{\bar{W}}$, Figures 9 and 10 already hint at the degree of complexity which the radiation may contribute to the problem. However, if the frequency range is changed, say, by altering the plate dimensions or materials, the radiation behavior also changes even if the vibration shapes stay the same. This is illustrated in Figures 11 and 12 where the radiation efficiency of the plates is shown for various frequency ranges. The frequency range is changed by means of a parameter, α, which proportionally shifts the frequency for the acoustic analysis up or down while the vibration response is kept unaltered.

From the figures above it can be seen that the radiation efficiency can easily vary by the same order of magnitude as the vibration response itself, thereby shaping the acoustic response in a critical manner. This is very pronounced in Case 2 where at low frequencies the radiation efficiency exhibits strong dips which almost cancel out the structural resonances and render the total sound power a rather smooth function. The reason for this lies in the fact that, because of the axially free boundary, there are no external forces

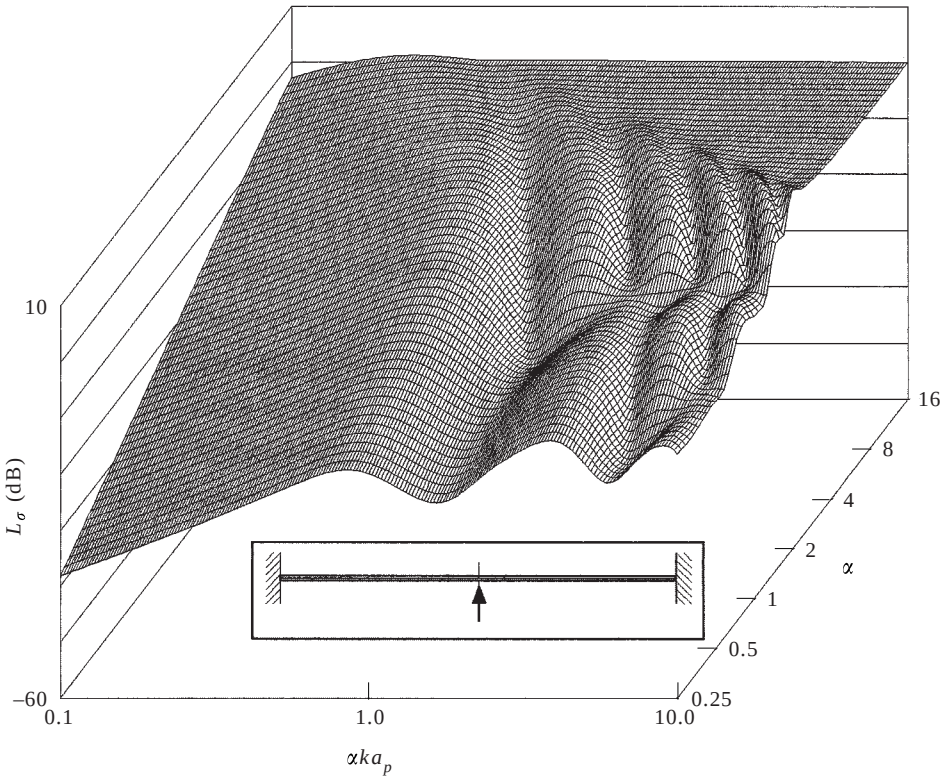

Figure 11. Radiation efficiency of clamped plate (Case 1) for various frequency ranges.

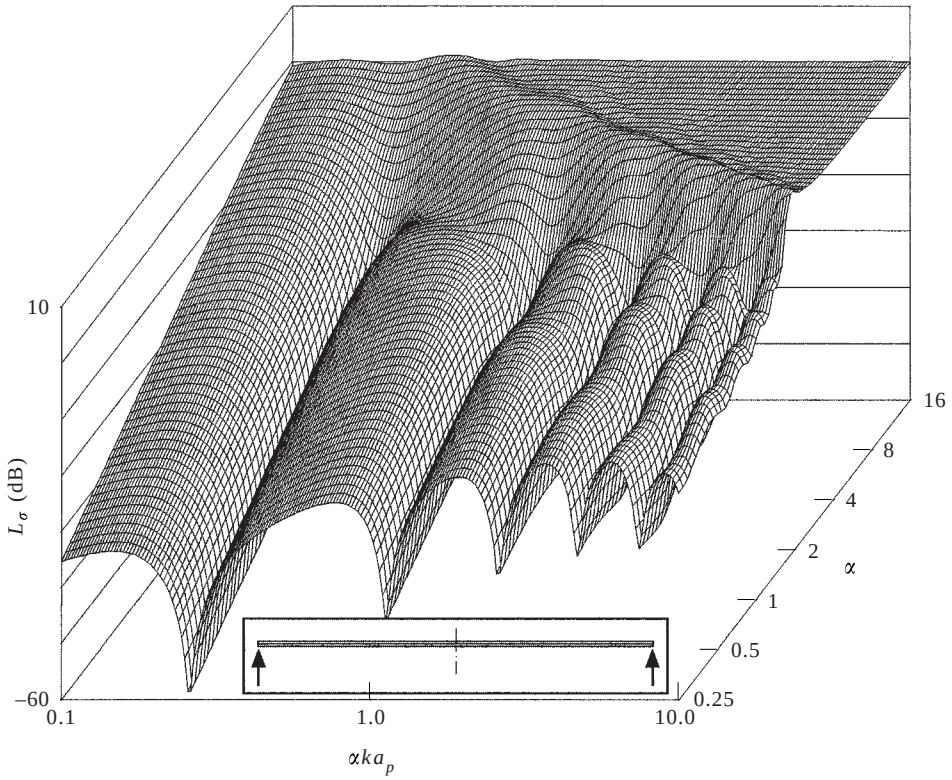

Figure 12. Radiation efficiency of free plate (Case 2) for various frequency ranges.

besides the excitation force. Since the excitation force amplitude is constant by definition, the acceleration amplitude of the mass center of the plate is also constant. Therefore, the plate's axial momentum cannot have resonances. The transverse momentum of a homogeneous thin plate in turn is directly proportional to its surface volume velocity,

$$U = \int_S v_n(r_s)\,\mathrm{d}S, \tag{19}$$

which, at low frequencies, predominantly determines the sound radiation. In contrast to this, high frequency radiation is governed by the surface average mean square velocity, meaning that the radiation efficiency approaches unity. However, as can be seen from Figures 11 and 12, this region is reached only with higher modes or high bending wave speeds: i.e., thick plates. The transition from the low to the high frequency range becomes more abrupt as the modal order increases.

With regard to the optimization of damping layer distributions, the inclusion of acoustic radiation increases the number of ways the objective function can be influenced. While minimizing vibration amplitudes focuses on damping enhancement as well as increasing stiffness, reducing radiated sound power can additionally utilize changes in vibration shapes and resonance frequencies. This leaves more potential for optimization, but also makes the objective function less smooth. Also, the maxima of the objective function no longer necessarily coincide with the structural resonances. However, it is assumed that

strong positive peaks of the radiation efficiency do not occur, so that the structural resonances still represent the overall optimization goal. This will be checked for the final design.

6.2. OPTIMIZATION

The initial design for the following examples is a uniformly coated plate with a damping layer thickness equal to the plate thickness (1 mm). Unless stated otherwise, in each example the first five resonances in the interval $ka_p = 0{\cdot}1 \cdots 10$ (36·39 Hz $\cdots$ 3639 Hz) are minimized simultaneously according to equation (3). Optimization is performed with respect to the summed A-weighted sound power level, L_{WA}, and, for comparison, with respect to the "simplified" A-weighted level, $L_{\bar{W}A}$, based on average mean square velocity only. The number of design variables (thickness points) is 10.

First, a clamped plate under a point load at the center (Case 1) is considered. The acoustic frequency response functions of the initial design (thinnest line in all figures) as well as of the optimized designs, both based on the full computational model, are shown in Figure 13 along with the corresponding damping layer distributions. The improvements achieved through optimization are given in parentheses in the fashion ($\Delta L^{i,j}_{\bar{W}A}$, $\Delta L^{i,j}_{WA}$), where i and j denote the lowest and highest resonance included in the optimization. As can be seen, both formulations of the objective function yield similar results. The minimization of $L_{\bar{W}A}$ delivers a slightly better solution, even for the true sound power. Obviously, the optimization with respect to L_{WA} suffers from the greater complexity of the objective function. (The algorithm monitors the Kuhn–Tucker conditions, but because of the very shallow target area optimization tends to terminate for numerical reasons, so that there is no exact proof for a true local optimum.) Started from the $L_{\bar{W}A}$-optimum, L_{WA}-minimization produces negligible further changes. The power reductions are achieved primarily by decreasing the average mean square velocity, while the radiation efficiencies at the resonance frequencies are slightly increased. However, the radiation efficiency in conjunction with the A-weighting determines which resonances are dominant.

A free plate excited at the rim (Case 2), is chosen for the next optimization example. Its radiation behavior, as seen in section 6·1, is quite different from that of a clamped plate. This particular behavior makes the initial design, a plate of constant thickness, almost optimal with respect to the radiated sound power. Hence, minimization of radiated sound power yields only very small changes in damping layer distribution (see Figure 14; the thinnest line of the initial design coincides with the thickest line of the Min L_{WA}-design almost everywhere). This is not so, however, if sound power based on average mean square velocity is minimized. Even though $L_{\bar{W}A}$is reduced considerably, the true radiated sound power is increased by 4·8 dB due to the changes in radiation efficiency: i.e., weakly radiating modes become better radiators. Although quite idealized, this example illustrates that applying a damping layer to a structure for noise reduction may have no effect or even a negative effect if not done properly.

In Case 3, the boundary conditions of the plate are more realistically chosen which makes the radiation behavior deviate from the acoustically ideal case discussed above. The first resonance of this configuration (piston-like mode) lies outside the frequency interval of interest and is therefore not considered. While the second mode still radiates weakly, the higher structural resonances are no longer matched by the radiation efficiency dips (see Figure 15). Minimizing $L_{\bar{W}A}$ yields more than a 10 dB reduction of the total average mean square velocity but only a 3 dB improvement in actual sound power. In contrast, minimization of L_{WA} lowers the radiated sound power by 5·7 dB although $L_{\bar{W}A}$ improves by only 3·7 dB. Lacking the radiation efficiency information, the $L_{\bar{W}A}$-minimization puts emphasis on the second resonance, thereby making the third mode a better radiator. This

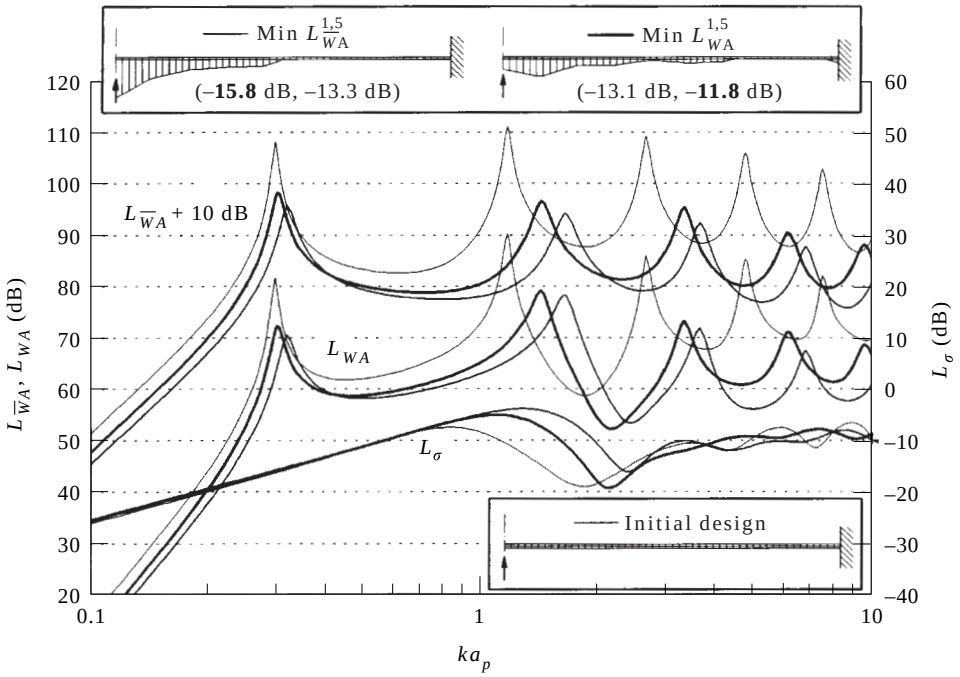

Figure 13. Acoustic freqeuncy response curves and damping layer distributions of initial and optimized designs (Case 1). $L_{\overline{WA}}$-curve lifted by 10 dB for clarity.

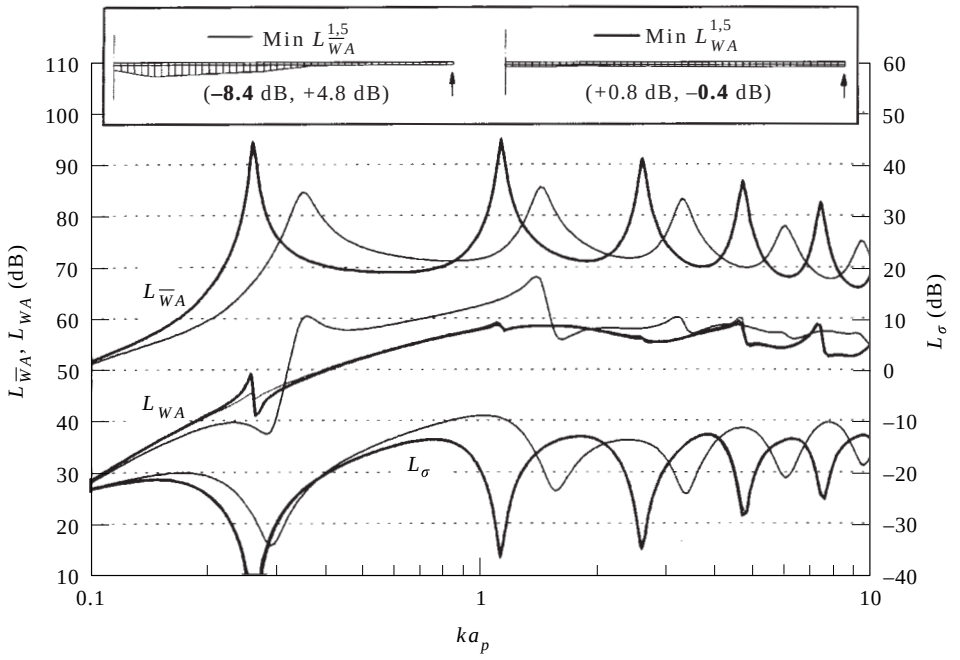

Figure 14. Acoustic frequency response curves and damping layer distributions of initial and optimized designs (Case 2).

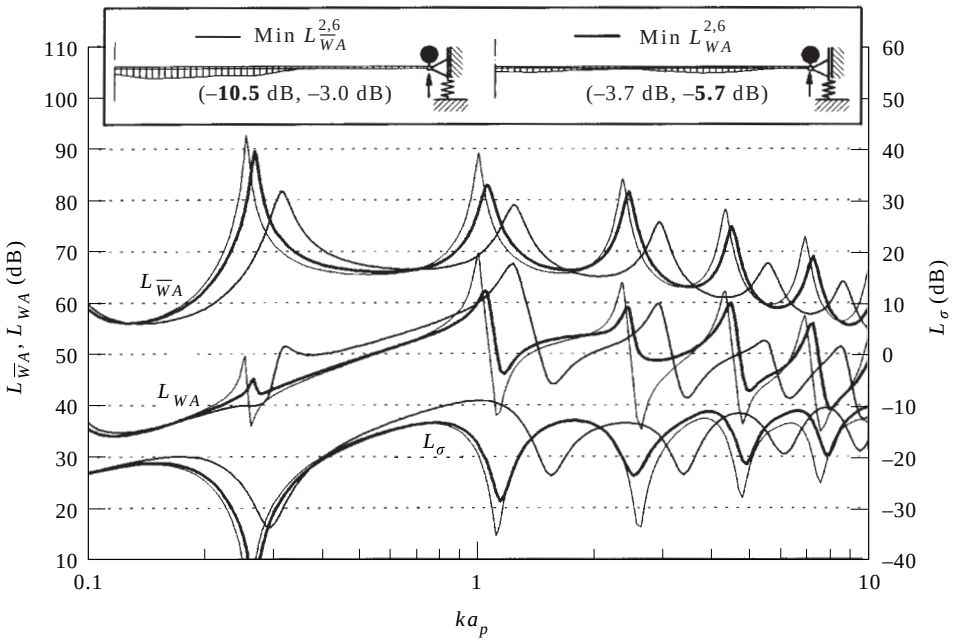

Figure 15. Acoustic frequency response curves and damping layer distributions of initial and optimized designs (Case 3).

still happens if the optimization is limited to the third resonance, as shown in Figure 16. However, minimizing L_{WA} of the third resonance alone yields a noticeable further reduction of that peak over the full-range optimization. This is mainly achieved by pulling the resonance peak and the radiation efficiency dip closer together.

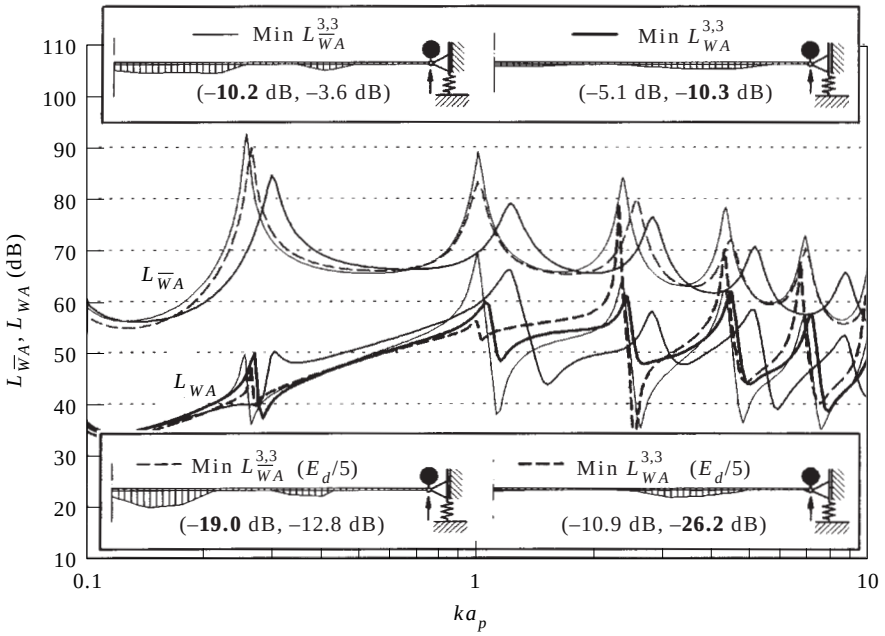

Figure 16. Acoustic frequency response curves and damping layer distributions of initial and optimized designs (Case 3). Optimized for third resonance only. E_d reduced to 20% in lower figures.

In order to elucidate the mode changing effect over the damping effect, more emphasis is put on the mass distribution by taking a different damping material, the Young's modulus of which is reduced to 20% of the original value (still frequency dependent). While minimization of $L_{\bar{W}A}$ (curve not shown to maintain clarity) leaves a peak similar to the initial design curve of the previous case, the softer damping material enables the L_{WA}-minimization to almost cancel the third resonance completely (see Figure 16) (note that the relative optimization gains in this case are much higher due to the softer damping material [29]). This low radiation efficiency of the third mode is achieved at the expense of the higher resonances, though.

7. CONCLUSIONS

With the example of circular plates, it has been shown that substantial reductions in broadband radiated sound power are possible by directed redistribution of damping layers. These reductions are due to several mechanisms which may be divided into "structural" effects and "acoustical" effects. The structural part primarily involves decreasing overall vibration amplitudes through an increase of damping and dynamic stiffness. While more damping lowers the resonance peaks, a higher dynamic stiffness reduces the response over a wider frequency band. Both effects require the damping layer to be concentrated where bending is highest (antinodes). However, if local stiffening becomes too great, the damping performance will decrease as the structure seeks to bend somewhere else.

In the low- and mid-frequency range, where structural wavelengths are smaller than or about equal to the wavelengths in the ambient medium, minimization of radiated sound power can utilize changes in vibration shapes and resonance frequencies to reduce radiation efficiency. These reductions are largely due to local source cancellations called acoustic short-circuit. As frequency increases, for example for thicker plates or higher modes (higher bending wave speeds), acoustic short-circuit effects become less significant until, at sufficiently high frequencies, the radiation efficiency approaches unity. Where achieving weakly radiating modes becomes an important factor, a means to produce those mode shapes directedly is desired. Redistribution of damping layers certainly bears this potential, as has been shown. However, stiffness and mass distribution cannot be modified independently which may lead to contradicting effects. Optimizing a combination of damping layer and lumped masses, for example, could help to overcome this problem.

Whether acoustic short-circuit effects can contribute significantly to a minimization of radiated sound power or not depends on the details of each particular problem (geometry, boundary conditions, frequency range, etc.). If such effects cannot be excluded or neglected *a priori*, they need to be taken into account since, as seen, applying or redistributing a damping layer may not always result in a reduction of sound power. In general, optimization gains will be greater if fewer modes must be included. Therefore, the effort of incorporating the radiation behavior can be beneficial in that it identifies radiationally dominant modes. However, it also increases complexity of the objective function and hence makes optimization more difficult. For more complex radiators, sound power calculations can become computationally very expensive. In order to simplify the optimization task in the low frequency range, one could consider minimizing the net surface volume velocity rather than solving the complete radiation problem.

Optimal solutions achieved with the method presented here are specific to the given excitation. Therefore, other forms of excitation like displacement excitation or acoustic excitation should be considered. Optimization with respect to a combination of load cases, for example a worst case scenario, is also conceivable. Frequency dependent loads can easily be incorporated. The general approach used in this paper is not limited to

unconstrained damping layers but can also be applied to other devices for vibration reduction. For systems with closely spaced resonances or stronger overall damping a refinement of the resonance tracking method will be necessary.

ACKNOWLEDGMENTS

The present work was greatly supported through a Feodor Lynen Research Fellowship awarded to H.-W. Wodtke by the Alexander von Humboldt Foundation, Germany, to which the authors are very grateful.

REFERENCES

1. A. D. Nashif, D. I. G. Jones and J. P. Henderson 1986 *Vibration Damping*. New York: John Wiley & Sons.
2. B. C. Nakra 1976/1981/1984 *Shock and Vibration Digest* **8**, 3–12/**13**, 17–20/**16**, 17–22. Vibration control with viscoelastic materials, Part I/Part II/Part III.
3. N. W. Hagood and A. von Flotow 1991 *Journal of Sound and Vibration* **146**, 243–268. Damping of structural vibrations with piezoelectric materials and passive electrical networks.
4. D. J. Mead and T. G. Pearce 1961 *University of Southampton*, *Department of Aeronautics and Astronautics*, *A.A.S.U. Report* 126. The optimum use of unconstrained damping layer treatments.
5. D. K. Rao 1978 *Acustica* **39**, 264–269.Vibration damping of tapered unconstrained beams.
6. K. K. Stevens, C. H. Kung and S. E. Dunn 1981 *Noise-Conference*, *North Carolina State University*, *Raleigh*, 445–452. Damping of plates by partial viscoelastic coatings, Part 1—analysis, Part 2—experimental evaluation. (Part 2 under Dunn, Kung, Jaising and Stevens).
7. G. Parthasarathy, C. V. R. Reddy and N. Ganesan 1985 *Journal of Sound and Vibration* **102**, 203–216. Partial coverage of rectangular plates by unconstrained layer damping treatments.
8. B. V. R. Gupta, S. Narayanan and N. Ganesan 1986 *Journal of Sound and Vibration* **105**, 517–521. Influence of applied damping treatment in different configurations on the overall damping of periodic structures.
9. A. Yildiz and K. Stevens 1985 *Journal of Sound and Vibration* **103**, 183–199. Optimum thickness distribution of unconstrained viscoelastic damping layer treatments for plates.
10. W. Suweca and L. Jezequel 1992 *International Journal for Numerical Methods in Engineering* **35**, 21–35. Optimal structural design with damping constraint limitations.
11. T. Lekszycki and N. Olhoff 1980 *The Danish Center for Applied Mathematics and Mechanics DCAMM Report* **195**. Optimal design of viscoelastic structures under forced steady state vibration.
12. T.-C. Lin and R. A. Scott 1987 *Proceedings of the* 58*th Symposium on Shock and Vibration*, *Huntsville*, *AL*, *NASA Conference Publications* **2488**, 395–409. Shape optimization of damping layers.
13. R. Lunden 1980 *Journal of Sound and Vibration* **72**, 391–409. Optimum distribution of additive damping for vibrating frames.
14. J.-L. Marcelin, Ph. Trompette and A. Smati 1992 *Finite Elements in Analysis and Design* **12**, 273–280. Optimal constrained layer damping with partial coverage.
15. J. C. McMunn and R. Plunkett 1969 *ASME Vibration Conference*, *Philadelphia*, *PA*, *ASME* 69-*VIBR*-42, 2–8. Multi-parameter optimum in linear dynamical systems.
16. H.-W. Wodtke, H. A. Eschenauer and J. S. Lamancusa 1993 *Advances in Design Automation*, Volume 2, *American Society of Mechanical Engineers*, **DE-Vol. 65–2**, 131–138. Layout of extensional surface damping treatment for minimal resonance response.
17. M. C. Junger and D. Feit 1993 *Sound*, *Structures*, *and Their Interaction*. Acoustical Society of America.
18. K. Naghshineh, G. H. Koopmann and A. D. Belegundu 1992 *Journal of the Acoustical Society of America* **92**, 841–854. Material tailoring of structures to achieve a minimum radiation condition.
19. J. S. Lamancusa 1993 *Computers and Structures* **48**, 661–675. Numerical optimization techniques for structural-acoustic design of rectangular panels.

20. R. L. St Pierre and G. H. Koopmann 1995 *ASME Journal of Vibration and Acoustics* **117** (special 50th anniversary design issue), 243–251. A design method for minimizing the sound power radiated from plates by adding optimally sized, discrete masses.
21. J. B. Oh 1993 *Ph.D. Thesis*, *Pennsylvania State University*. An efficient method for designing quiet composite structures via material tailoring.
22. E. L. Wilson, R. L. Taylor, W. P. Doherty and J. Ghaboussi 1973 in *Numerical and Computer Methods in Structural Mechanics* (S. J. Fenves *et al*., editors). New York: Academic Press. Incompatible displacement models.
23. D. R. Bland 1960 *The Theory of Linear Viscoelasticity*. New York: Pergamon Press.
24. H. Eschenauer, J. Koski and A. Osyczka (editors) 1990 *Multicriteria Design Optimization*. Berlin: Springer.
25. E. J. Haug and J. S. Arora 1979 *Applied Optimal Design*. New York: John Wiley & Sons.
26. G. V. Reklaitis, A. Ravindran and K. M. Ragsdell 1983 *Engineering Optimization*, *Methods and Applications*. New York: John Wiley & Sons.
27. A. Parkinson and M. Wilson 1986 *ASME Design Engineering Technical Conference*, *Columbus*, *OH*, *ASME* 86-*DET*-114. Development of a hybrid SQP-GRG algorithm for constrained nonlinear programming.
28. H. A. Eschenauer, J. Geilen and H. J. Wahl 1993 SAPOP—an optimization procedure for multicriteria structural design. In *International Series of Numerical Mathematics*, Volume **110**, 207–227 (H. R. E. M. Hörnlein and K. Schittkowski, editors). Basel: Birkhäuser. Software systems for structural optimization.
29. H.-W. Wodtke 1992 *Ph.D. Thesis*, *University of Siegen*, *FOMAAS*, *TIM-Forschungsberichte*, T01-09.92. Optimale Auslegung von Dämpfungsbelägen zur Schwingungsreduzierung.